International Journal of Scientific Engineering and Research (IJSER)
ISSN (Online): 2347-3878
Index Copernicus Value (2015): 62.86 | Impact Factor (2015): 3.791

Effect of Slag as a Fine Aggregate on Mechanical, Corrosion, and Nuclear Attenuation Properties of Concrete

R. M. El Shazly[1], M.M. Sadawy[2]

[1]Physics Department, Faculty of Science, Al-Azhar University, Nasr City, Cairo 11884, Egypt.

[2]Mining and Petroleum Engineering Department, Al-Azhar University, Nasr City, Cairo 11371, Egypt.

Abstract: ***A series of concrete maxis were designed and prepared by replacement percentages (0, 5, 10, and 20 wt%) of their fine aggregates by blast furnace slag. Mechanical properties, corrosion in the steel reinforcement, and different types of Nuclear radiation parameters of four concrete maxis were studied. The corrosion behavior was investigated using different electrochemical techniques and optical microscope. Also, three types of neutron energies as well as nine gamma ray energy lines (121.78 – 1407.92 keV) were used to evaluate the macroscopic neutron cross-sections (Σ, cm^{-1}) and mass attenuation coefficients (σ, cm^2/g) of gamma ray, respectively, in investigated concrete samples. The results showed that, the mechanical properties of concrete and the corrosion resistance of steel imbedded in concrete were increased with increasing blast furnace slag up to 10 wt. %. While, 20 wt % was the optimum percentage for the values of mass attenuation coefficients of most investigated γ-ray energy lines in concrete maxis. Moreover, there is no a significant variation of the values of Σ for all used neutron energy by adding a different percentage of slag as a fine aggregate in concrete.***

Keywords: Blast furnace slag in concrete, Corrosion, Neutron macroscopic cross-section, Mass attenuation coefficient

1. Introduction

The choice of materials for radiation shield design depends essentially on neutrons and gamma rays where the materials capable of attenuating these types of radiations to acceptable level will automatically reduce all other radiation types to negligible extent. Also, the cost and efficiency of the materials are important factors for shield design. As well as the above reasons Concrete considered a good shield where it solves difficulties of collecting a heavy and light element in the same shield [1]-[4]. To improve the attenuation properties of concrete for neutrons and gamma-rays it will be designed and fabricated in especial way to also, maintain its original strength and durability against pressures and tensions [5]. Moreover, demand for concrete as a construction material is growing day by day [6]-[10]. The average world production of concrete in our rapid developing industrialized world is about 6 billion tons per year [6]. Since earth is the source of the aggregates either natural or crushed material. These amounts would have an adverse effect on the environment [7]. For normal concrete, aggregates consist of sand, gravel, and crushed stone which are vital elements in concrete industry. Sand as a fine aggregate is mined from river beds and open pits. With the launching of major infrastructure projects and continuous developments in construction industry, there is an extraordinary increase in the demand for sand in many developing countries. However, sand mining is becoming a severe ecological issue, in various parts of the world, due to the number of environment-related issues like reduction in water head leading to less recharging of water into the ground aquifers, wearing down of land, disturbance due to excavating of sand and lifting [9]. Therefore, the search for natural aggregate replacement has become an important and urgent issue to preserve the natural resources and helps to promote sustainable development in the protection of natural resources.

Blast furnace slag, a by-product from the steel-making process, is made by rapid cooling of a slag melt of suitable composition, as obtained by smelting iron ore in a blast furnace and contains at least two-thirds by mass of glassy slag and possesses hydraulic properties when suitably activated. Granulated blast furnace slag consists of at least two-thirds by mass of the sum of calcium oxide (CaO), magnesium oxide (MgO), and silicon dioxide (SiO_2). The remainder contains aluminum oxide (Al_2O_3) together with small amounts of other compounds [10].

As a matter of fact, for many years ground granulated blast furnace slag (GGBS) has been used as a supplementary cementitious material in concrete, either as a mineral admixture or a component of blended cement. Chen et al. [11] found that the high slag blast furnace cement (HBFC) concretes had lower porosity than the corresponding ordinary Portland cement (OPC) concretes with the same design strength. As well as HBFC concretes showed considerably better resistance to chlorides ion penetration than the OPC concretes. Sharmila, and Dhinakaran [12] demonstrated that ultra-fine slag has enhanced the compressive strength and durability characteristics of high strength concrete. Aleksander Samarin [13] indicated that the attenuation differences of dense and ordinary concretes can be significantly affected by the specific selection of aggregate and by the mix composition. Also, found that the attenuation of the intensity of radiation by the factor of 10 For high density concrete is better than that of water and ordinary concrete.

The objective of this research is to investigate the effect of blast furnace slag as a fine aggregate on mechanical, corrosion and nuclear attenuation behaviors of concrete.

2. Experimental Work

2.1 Materials

2.1.1 Cement

The present study was carried out using a commercial Portland cement type CEM I 42.5 N conforming to Egyptian standard code ESS 2421/2007. The physical, chemical and mechanical properties of this cement are given in Table no 1

Table 1: Properties of Cement Type (CEM I 42.5 N)

Chemical	Composition (wt.%)	Physical properties	Compressive strength (N/mm^2)
SiO_2	20.36	Fineness (cm^2/gm) 3290	2 days 22.4
Al_2O_3	5.12	Specific Gravity 3.15	7 days 33.7
Fe_2O_3	3.64	Expansion (mm) 1.2	28 days 56.8
CaO	63.39		
MgO	1.03		
SO_3	2.21		
L.O.I	1.3		

2.1.2 Blast furnace slag

The blast furnace slag was supplied from Egyptian Iron and Steel Company, Helwan, Egypt. It was air-cooled slag and produced as a by-product through iron and steel making. Its chemical composition is shown in Table no. 2.

Table 2: Chemical composition (wt %) of blast furnace slag

SiO_2	Al_2O_3	Fe_2O_3	CaO	MgO	MnO	P_2O_5	SO_3
38.13	7.98	0.43	39.9	9.23	1.42	0.14	0.18

2.1.3 Aggregates

Natural siliceous sand having a fineness modulus of 2.66 and a specific gravity of 2.67 was used as fine aggregate. The coarse aggregate was a crushed dolomite with a maximum nominal size of 18 mm with a specific gravity of 2.64 and a crushing modulus of 23 percent.

2.1.4 Steel

High tensile ribbed steel bars of 12 mm diameter were cut into 20 cm. its chemical composition is shown in Table no. 3.

Table 3: Chemical composition (wt %) of steel bars.

C	Si	Mn	Ni	Cr	Mo	Fe
0.39	1.43	0.55	1.62	0.70	0.32	Bal.

2.1.5 Water

The water used was clean, fresh, free from impurities, and was taken from portable water supplies.

2.2 Mixing and casting

Concrete mixes were prepared using a tilting drum mixer. The weighted coarse and fine aggregates were placed in the mixer and started mixing for 30 seconds to obtain a homogeneous mix. The cementitious materials were added to the mixer and stirred for 2 min. The water was slowly added and mixed for 2 min. The mixing process was continued for 3 min. Under a laboratory conditions, six cubes of 150 mm and six cylinders of 150 × 300 mm were prepared and compacted by a vibrating rod. For the corrosion tests, steel bars were cleaned with ethanol and then dried prior to embedding in the center of 150 mm cube mold at a cover of 25 mm. After casting, all specimens were covered with plastic sheet and stored in the laboratory for 24 hours. The specimens were then demolded, and placed in water for 28 days. Moreover, one of the prepared cylinder was cut off by thickness varies from 3.5 up to 20 cm for nuclear radiation (γ-rays and neutrons) measurements.

2.3 Fresh properties of concrete mixes

The consistency and workability of the concrete mixes was evaluated using the slump cone test.

2.4 Mechanical tests

Compressive strength tests on cubes at 3, 7 and 28 days were carried out in a compression testing machine. The cubes were fitted and the load was slowly applied. The tensile strength tests were performed on cured cylinders specimen at 28 days.

2.5 Electrochemical corrosion tests

The electrochemical corrosion tests were performed using a Potentiostat/ Galvanostat (EG&G model 273). M352 corrosion software from EG&G Princeton Applied Research was used. A three-electrode cell composed of a concrete specimen as a working electrode, Pt counter electrode, and Ag/AgCl reference electrode were used for the tests (see Fig.1). The open-circuit potential (OCP) was recorded after immersion of the samples in the test solution for 60 days vs. Ag/AgCl reference electrode. Potentiodynamic polarization tests at scan rate of 0.5 mV/s were carried out. PAR Calc Tafel Analysis was used to fit the experimental data. Cyclic potentiodynamic tests were performed by scanning the potential in the forward direction from -100 mV Ag/AgCl towards the anodic direction at a scan rate of 1.0 mV/s. The potential scan was reversed when the current density reached a value of 0.10 A/cm^2. Before tests each water-cured specimen was taken from water and then rubbed with a clean dry cloth until a dry surface sample was obtained. All solutions were freshly prepared from analytical grade chemical reagents using distilled water.

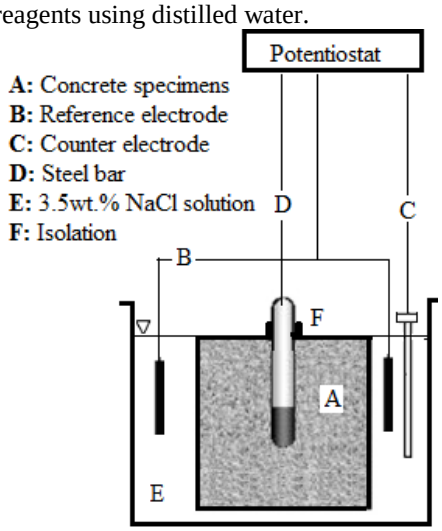

Figure 1: Experimental setup of electrochemical corrosion measurement

2.6 Microstructure Analysis

X-ray diffraction (XRD, Philips Analytical X-ray B.V. Machine) and scanning electron microscope (SEM, Joel-JXA-840A) have been used to investigate the structure of concrete with and without blast furnace slag. All concrete samples were coated with gold to improve the appearance of microstructure.

2.7 Neutron and gamma ray measurements and calculations

The BF_3 neutron detector was used to detect a collimated slow neutron, total slow neutron, and neutron with energy greater than 10 keV beam emitted from ^{241}Am-Be neutron source with activity 3.7 GBq. the neutron transmitted fluxes were measured according to equation (1) [14] to deduce the values of macroscopic neutron cross-section. In case of slow neutrons measurements, the collimated beam was slowed down by 7 cm polyethylene block behind the sample, also the neutron of energy below 10 keV was cut off by a block of Born carbide B_4C. the Schematic diagram of experimental setup was shown in Fig. 2.

$$I = I_o\, e^{-\Sigma x} \tag{1}$$

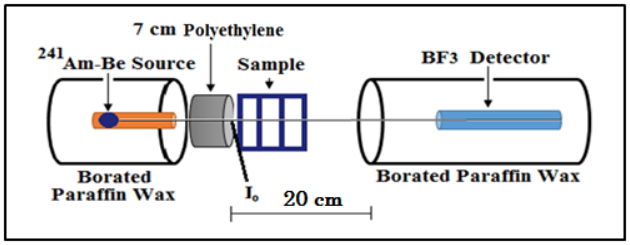

Figure 2: Schematic diagram of Neutron spectrometer

A collimated beams of gamma rays emitted from 3.7 μCi Eu-152, 9.5 μCi Cs-137, and 4.9 μCi Co-60 radioactive sources were used as a sources of gamma ray energies. Nine pronounced peaks from the energy spectrum of gamma rays were chosen to cover a wide band of gamma energies to study the gamma ray attenuation coefficients of the investigated concrete barriers. Fig. 3 showed the schematic diagram of gamma ray detection system, where a 3″ x 3″ NaI(Tl) scintillation detector was used to measure the gamma ray intensities for the studied energy lines. The Beer-Lambert's equation was used to evaluate the linear attenuation coefficient, which considered the basic nuclear parameter, depending on the gamma ray intensities that transmitted from the investigated samples [15],[16].

$$\mu = \frac{\ln(\frac{I}{I_o})}{x} \tag{2}$$

Where, I_o & I are the intensities of gamma rays before and after transmitted the sample, respectively, μ (by cm^{-1}) is the linear attenuation coefficient of the sample, and x is the thickness of the sample. Mass attenuation coefficient, σ (by cm^2/g) is another important nuclear parameter which independent of density of the material, was evaluated from equation (3) after considering superficial density (xρ) in states of thickness;

$$\sigma = \frac{\ln(\frac{I}{I_o})}{x\rho} \tag{3}$$

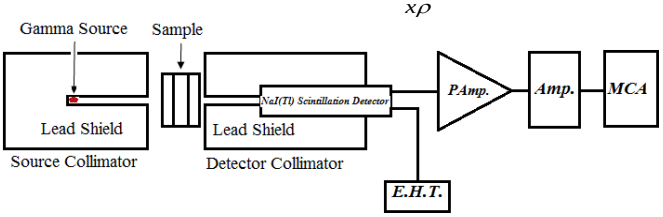

Figure 3: Schematic diagram of experimental setup for gamma ray detection

The comparison between experimental and theoretical data was carried out by using the WinXCom computer program (version 3.1) [17],[18],[19] to calculate the mass attenuation coefficients of γ-rays of such used energies for the studied concrete samples based on the mixture rule of the following equation:

$$\sigma_{Th} = \sum_i^n W_i (\frac{\mu_i}{\rho_i})_m \tag{4}$$

Where, $(\mu_i/\rho_i)_m$ is the mass attenuation coefficient for the individual element in each mixture sample, W_i is the fraction weight of the element in each mixture sample.

The maximum error in attenuation coefficients was evaluated using the following propagation of error formula [16],[20]:

$$\Delta\sigma = \frac{1}{x\rho}\sqrt{(\frac{\Delta I_o}{I_o})^2 + (\frac{\Delta I}{I})^2 + (\ln\frac{I_o}{I})^2(\frac{\Delta x\rho}{x\rho})^2} \tag{5}$$

3. Results and Discussions

3.1 Fresh concrete

The slumps of fresh concrete for different mixtures were shown in Fig. 4. It was noticed that the slump test values were decreased with increasing slag content in concrete. This behavior was probably due to the rough texture and high-water absorption of slag particles, leading to low fluidity.

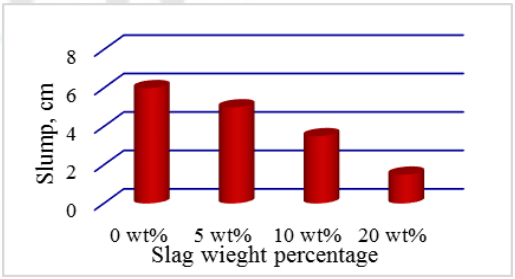

Figure 4: Effect of slag as a fine aggregate on slump value.

3.2 XRD diffraction patterns

The X-ray diffractograms of concrete with and without slag after 28 days are shown in Fig.5. Analysis of the patterns indicates the presence of lines corresponding to phases of Portlandite $Ca(OH)_2$, tri-calcium silicate hydrate (C_3SH), alpha di-calcium silicate hydrate (α-C_2SH), calcite ($CaCO_3$), calcium silicate hydrate (C-S-H) and SiO_2. It is obvious from Fig. 5 that the peaks of portlandite (CH) decreased while the peaks of C-S-H markedly increased with increasing slag content. This behavior was due to the pozzolanic reaction of slag with the liberated lime, which forms additional amount

of C-S-H. Moreover, the XRD patterns show that $CaCO_3$ peaks decrease with increasing slag. This was due to the decrease of Portlandite in concrete.

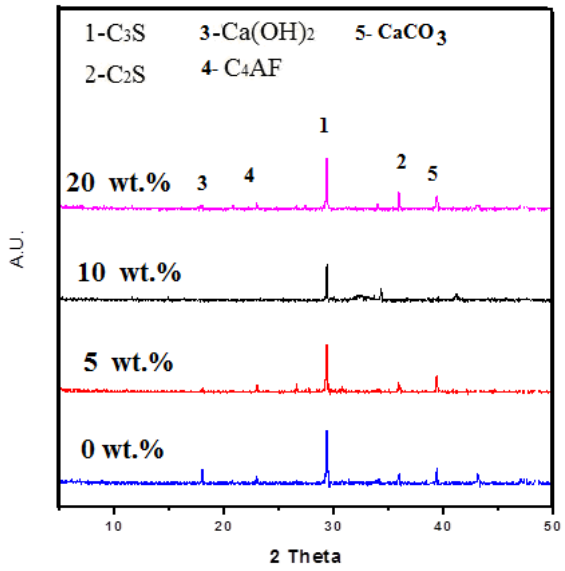

Figure 5: XRD diffraction of concrete with and without slag as a fine aggregate.

3.3 Microstructure (SEM) analysis of the hydrated concrete

Fig. 6 (a-d) shows microstructure of concrete with and without slag. It can be seen that the plain concrete has more voids comparing to concrete with slag. In addition, the figure revealed that the voids decreased with increasing slag content to 10 wt.%. Beyond this value the voids increased again, but still lower than both the plain and 5wt.% specimens. On the other hand, Fig. 6 displays that the internal structure of slag concrete was similar to the structure of Portland cement concrete without slag.

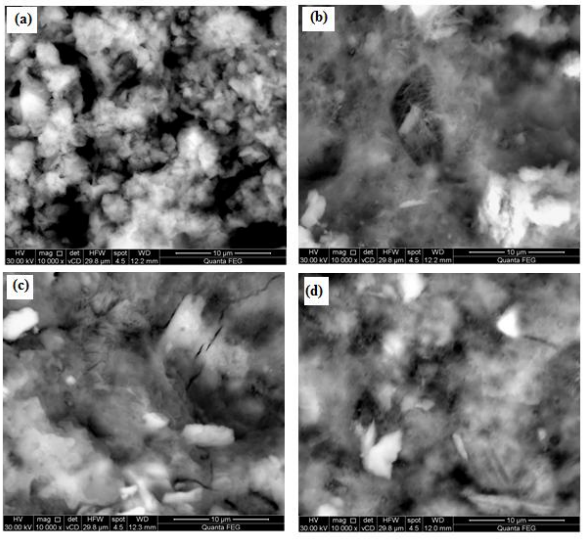

Figure 6: Microstructure of concrete with and without slag as a fine aggregate. (a) concrete without slag, (b) 5wt.% slag, (c) 10 wt.% slag and (d) 20wt.% slag.

3.4 Mechanical properties of hardened concrete

3.4.1 Compressive strength

Fig. 7 presents the compressive strength of concrete with and without slag as fine aggregate after 3, 7 and 28 days of curing. The results revealed that the compressive strength for all concrete mixes increased with the curing time. This was mainly attributed to the cement hydration and accumulation of hydration products which close some of available pore spaces in concrete matrix and result in improving the mechanical performance. Furthermore, Fig. 7 indicated that the compressive strength increased by adding slag up to 10 wt% replacements. Beyond this value the compressive strength decreased, but still more than the control specimen. This reduction in compressive strength for concrete mix with 20 wt% replacement was due to the decrease in the free water content that resulted from the high-water absorption characteristics of blast furnace slag in comparison with sand (see Fig. 4). This causes a considerable decrease in the workability of concrete and hence, increase the voids in this mix.

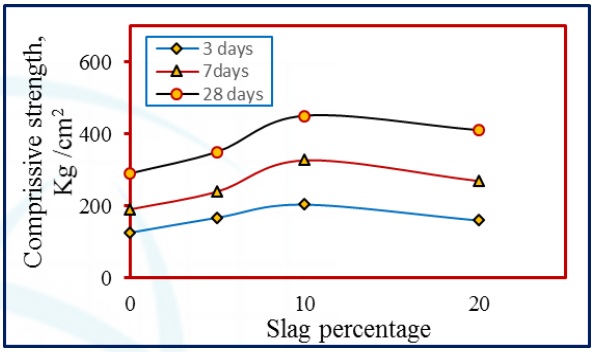

Figure 7: Effect of slag as a fine aggregate on compressive strength of concrete.

3.4.2 Splitting tensile strength

Fig. 8 depicts the results for splitting tensile strength of different slag mixes concrete. It was noticed that all slag mixes have gained higher split tensile strength than that of the control mix. However, beyond 10 wt% replacement the tensile strength decreases, but still more than the control mix. The trend was similar to the trend of compressive strength development of concrete. This behavior was due to decreasing the cementitious material per surface area of fine aggregate and increasing the voids beyond this value.

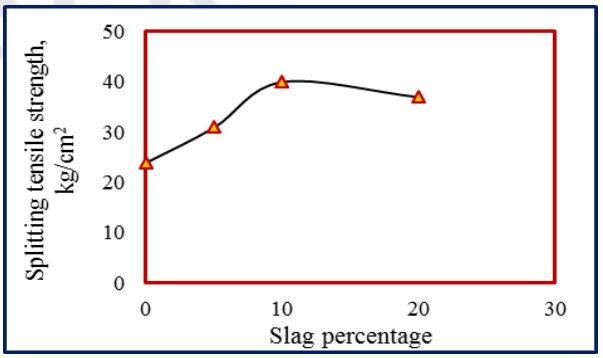

Figure 8: Effect of slag as a fine aggregate on tensile strength of concrete

3.5 Effect of blast furnace slag on corrosion of reinforced steel bars imbedded in concrete

3.5.1. Open circuit potential (OCP)

The development of OCP for steel bars in concrete with different slag content as fine aggregate is shown in Fig. 9. The results showed that replacing sand with increasing

proportions of blast furnace slag up to 10% wt. has increased the OCP in the positive direction. However, when the proportion of slag was more than 10% wt. the OCP shifted to negative direction. This was not surprising because it was expected that such a high replacement level decreased the free water content that resulted from the high-water absorption characteristics of slag, resulting in a less dense internal structure and more interconnected pores that would facilitate ion mobility. Thus, the OCP shifted in the negative direction.

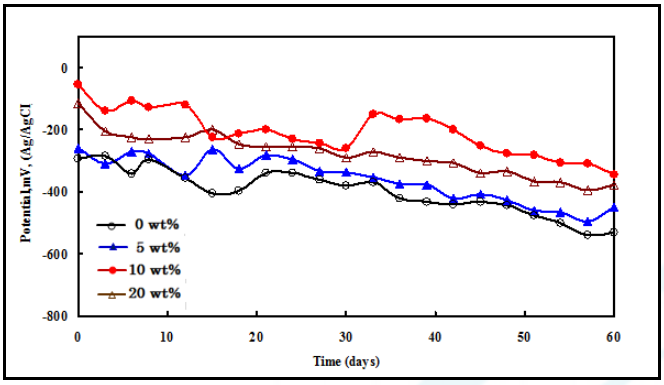

Figure 9: Potential–time curves of steel imbedded in concrete with and without slag as a fine aggregate in 3.5 wt. % NaCl solution.

3.5.2. Potentiodynamic polarization

Potentiodynamic polarization curves of steel imbedded in concrete with and without blast furnace slag are shown in Fig.10. All samples were immersed in 3.5 wt. % NaCl solution for 15 days before polarization tests to achieve their stable OCP values. The anodic polarization curves show that increasing slag content to 10 wt. % as fine aggregate replacement, the corrosion potential (E_{cor}) shifts to more noble potential and the corrosion rate decreases from 878.4 to 3.752 µA/cm^2. This behavior may be attributed to decreasing the pore size in concrete, leading to decreasing the chloride ions mobility. The electrochemical parameters including corrosion potential (E_{corr}), corrosion current density (i_{corr}), anodic and cathodic slopes (β_a and β_c) were calculated and summarized in Table no. 4. The data in Table no. 4 revealed that the anodic and cathodic Tafel slopes changes with increasing slag content. This means that blast furnace slag has obvious effect on anodic and cathodic reactions.

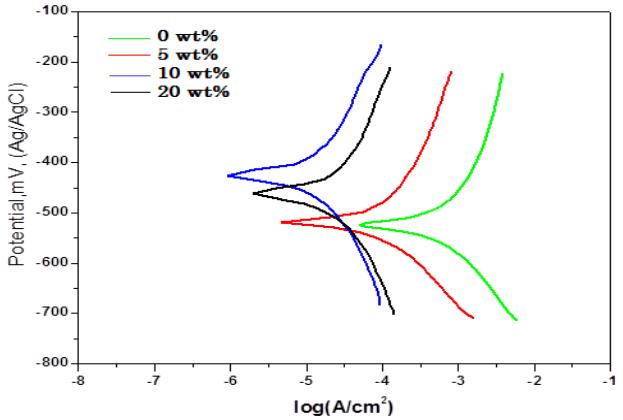

Figure 10: Tafel polarization curves of steel imbedded in concrete with and without slag as a fine aggregate in 3.5 % Nacl solution.

Table 4: Corrosion parameters of steel imbedded in concrete with and without slag as a fine aggregate in 3.5 wt. % NaCl solution.

Slag, wt. %	$E_{cor.}$ (mV)	i_{cor} (µA/cm^2)	β_c (mV/dec)	β_a (mV/dec)
0	-535	878.4	159.3	188.5
5	-520	250.9	79.4	143.8
10	-430	3.752	54.4	90,5
20	-450	15.56	53.7	91.5

3.5.3. Cyclic polarization

In order to investigate the effect of blast furnace slag as fine aggregate on pitting and passive stability of steel imbedded in concrete contaminated with chloride ions, the cyclic polarization technique was used as shown in Fig.11 It is obvious from Fig.11 that the obtained plots had the familiar shape of steel in concrete, showing a well-defined corrosion potential followed by a passive region. The passive region was due to the formation of a protective barrier oxide film which was formed in high pH environment. Moreover, Fig.11 indicated that the passive region increased with increasing slag content to 10 wt.% as fine aggregate replacement. This was due to the rapid consumption of crystalline $Ca(OH)_2$ which were quickly formed during early hydration and formation of excessive amounts of hydrated compounds of calcium silicate [21]. These compounds were expected to react with the pore solution to form additional gel. The action of the newly formed gels was directed into the improvement of the densification, pore refinement and chemical–mechanical stability of the matrix [22]. On the other hand, Fig.11 indicated that the passive region decreased, but still more than the control specimen, by replacing slag more than 10 wt%. This behavior may be attributed to the high-water absorption of slag. Hence the chloride ions increased in interconnected pores, leading to a destructive of the passive zone in steel.

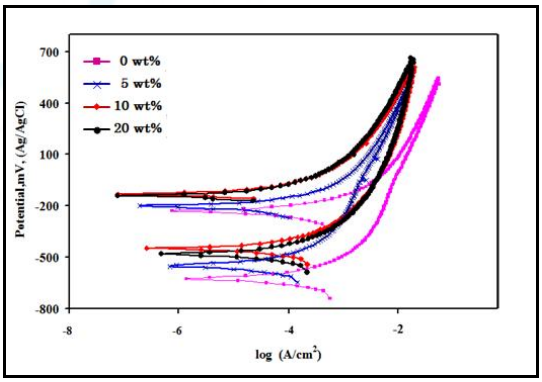

Figure 11: Cyclic polarization curves of steel imbedded in concrete with and without slag as a fine aggregate in 3.5 wt. % NaCl solution

3.5 Neutron measurements

The values of removal cross-sections of total slow neutrons (E_{n1}) (primary slow as well as slowdown in the studied concrete mixes), slow (E_{n2}), and neutron with energy greater than 10 keV (E_{n3}) were deduced from attenuation curves and shown in Table no. 5. It was observed that, the values of macroscopic cross-sections of slow neutrons in all types of concrete under investigation were the biggest values of the others neutron energies. This behavior of slow neutrons may

be attributed to elastic scattering of slow neutron with light elements in all types of concrete mixes. Also, it was noticed that the values of macroscopic cross-sections of total slow neutron slightly increasing than that of neutron with energy greater than 10 keV in all concrete mixes. This behavior may be attributed to the competition between absorption process and slowdown process which takes place in the case of total slow neutron, while in the case of neutron with energy greater than 10 keV the only slow down process that appear. (note that, about 23% of neutron energies emitted from ^{241}Am-Be neutron source is considered slow neutron). Also, it was observed from Table no. 5 that the values of macroscopic cross-sections of all used neutron energies almost constant with increasing the percentage weight of slag in concrete mixes. This result can be interpreted as, the addition of slag up to 20 wt% as a fine aggregate in the concrete decreased the percentage of SiO_2 and in the same time increased the percentage of CaO as well as another element composition nearly don't change as in Table no. 6.

Table 5: Macroscopic cross-sections of concrete mixes at different neutron energies

N	Macroscopic cross-section, cm^{-1}			
	0%	5%	10%	20%
E_{n1}	0.049 ± 0.0034	0.050 ± 0.0034	0.048 ± 0.0036	0.047 ± 0.0027
E_{n2}	0.091 ± 0.0044	0.092 ± 0.0047	0.092 ± 0.0045	0.091 ± 0.0032
E_{n3}	0.041 ± 0.0032	0.043 ± 0.0047	0.044 ± 0.0039	0.042 ± 0.0044

Table 6: Chemical composition and density of concrete mixes

Concrete Mixes	Chemical composition, wt%						Density $gm.cm^{-3}$
	SiO_2	Al_2O_3	Fe_2O_3	CaO	MgO	SO_3	
0 wt%	0.412	0.025	0.015	0.427	0.114	0.008	2.3862
5 wt%	0.401	0.026	0.015	0.435	0.115	0.008	2.4010
10 wt%	0.391	0.027	0.015	0.443	0.117	0.008	2.3822
20 wt%	0.362	0.030	0.015	0.464	0.122	0.008	2.4109

Also, the comparison of half value layers of different types of investigated concrete mixes for different neutron energies was shown in Table no. 7.

Table 7: Half value layer (HVL) of all investigated samples at different neutron energies.

N	HVL, cm			
	0%	5%	10%	20%
E_{n1}	14.15 ± 0.69	13.86 ± 0.66	14.44 ± 0.76	14.75 ± 0.58
E_{n2}	07.62 ± 0.26	07.54 ± 0.21	07.54 ± 0.26	07.62 ± 0.19
E_{n3}	16.91 ± 0.92	16.12 ± 1.22	15.76 ± 0.97	16.51 ± 1.20

3.7 Gamma-rays measurements and calculations

The intensity distribution of gamma rays transmitted through concrete barriers of different thicknesses were measured and plotted at different percentage of slag as a fine aggregate and at different incident gamma ray energy lines (121.78, 344.27, 661.64, 778.9, 964, 1112.4, 1173.23, 1332.51, 1407.92 keV). These exponential curves were used to deduce the total linear attenuation coefficients (μ, cm^{-1}) as a slope of these curves. Fig. 12 (a-d) showed the behavior of measured and calculated mass attenuation coefficient (σ, cm^2/g) with obtained gamma ray energies. The first note of these curves was a good agreement between the measured values of mass attenuation coefficients and that calculated by winXCom computer program (version 3.1), especially in the energy range of 344 - 1407 keV. Also, the behavior of all these curves can be interpret by the prominent interaction between the investigated concrete barriers and gamma rays which considered a Compton scattering process as well as less contribution of photoelectric effect in low energies.

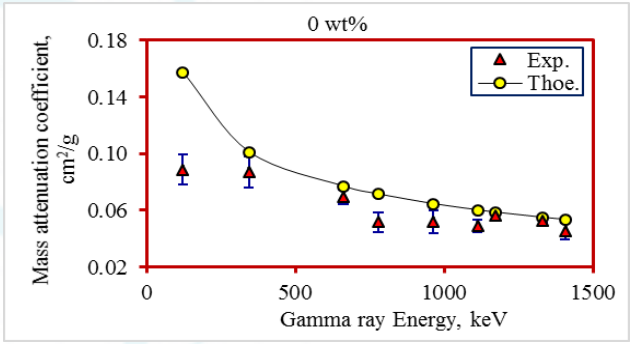

(a)

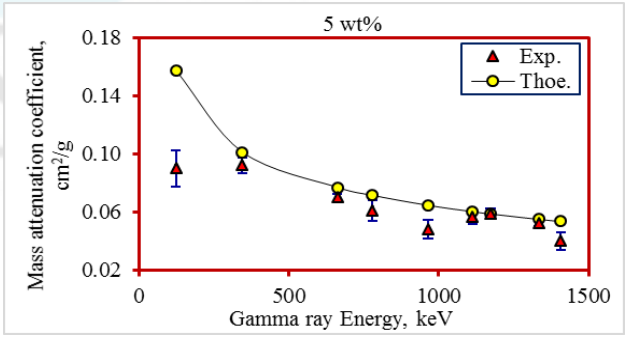

(b)

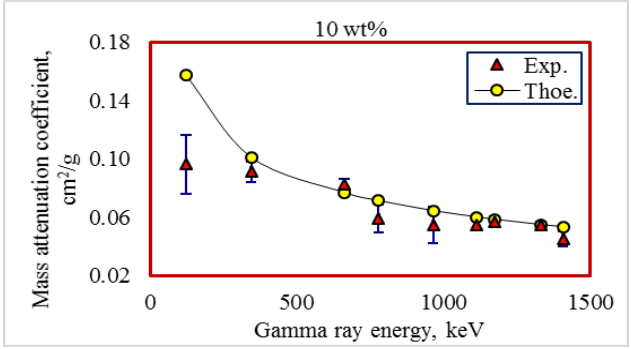

(c)

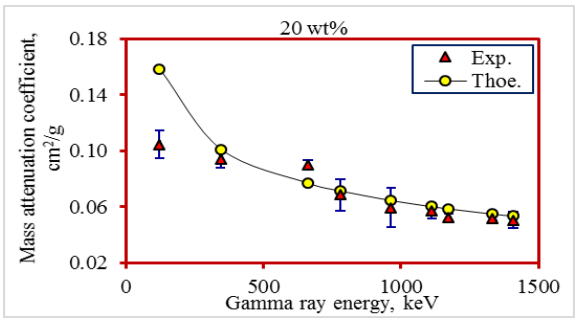

(d)

Figure 12: Mass attenuation coefficients of concrete with and without slag as a fine aggregate. (a) concrete without slag, (b) 5 wt.%, (c) 10 wt.%, and (d) 20 wt.%.

Fig. 13 showed the comparison between values of mass attenuation coefficients in different types of investigated concrete mixes and used gamma ray energies. The basic feature of this figure was that, the values of σ (by cm^2/g) were increased by increasing the weight percentage of slag as a fine aggregate in concrete mixes up to 1112.4 keV gamma ray energy, which may be attributed to Z-dependence of Compton scattering process in this energy region. While for another gamma ray energies there is a fluctuation distribution of values of mass attenuation coefficient.

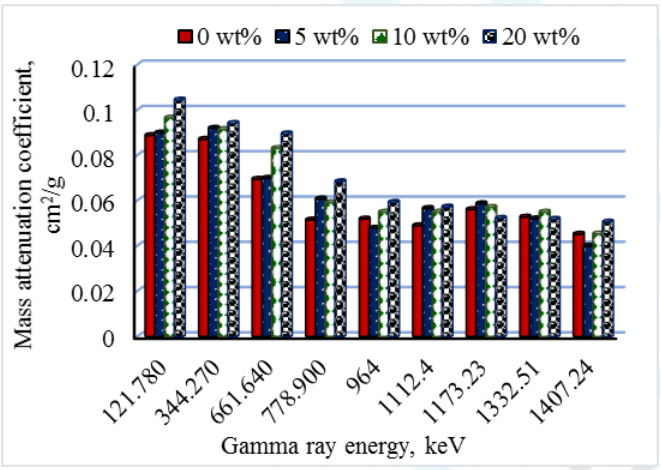

Figure 13: Comparison between mass attenuation coefficients of investigated concrete mixes with different gamma ray energies.

The comparison of half value layers of different types of investigated concrete mixes for different used gamma ray energies was shown in Table no. 8.

Table 8: Half value layer (HVL) of all investigated samples at different gamma ray energies

γ-Energy, keV	HVL, cm			
	0%	5%	10%	20%
121.78	3.27 ± 0.27	3.21 ± 0.31	3.01 ± 0.44	2.75 ± 0.18
344.27	3.33 ± 0.29	3.12 ± 0.12	3.18 ± 0.25	3.05 ± 0.21
661.64	4.18 ± 0.17	4.13 ± 0.09	3.50 ± 0.10	3.21 ± 0.10
778.9	5.64 ± 0.55	4.75 ± 0.40	4.92 ± 0.54	4.20 ± 0.65
964	5.60 ± 0.62	6.03 ± 0.55	5.29 ± 0.82	4.85 ± 0.78
1112.4	5.93 ± 0.34	5.10 ± 0.31	5.29 ± 0.27	5.02 ± 0.41
1173.23	5.17 ± 0.16	4.92 ± 0.19	5.10 ± 0.19	5.50 ± 0.19
1332.51	5.50 ± 0.12	5.55 ± 0.11	5.29 ± 0.15	5.55 ± 0.15
1407.24	6.42 ± 0.56	7.22 ± 0.77	6.42 ± 0.54	5.68 ± 0.62

4. Conclusion

- The mechanical properties of concrete and the corrosion resistance of steel imbedded in concrete were increased with increasing blast furnace slag up to 10 wt. % as a fine aggregate. Beyond this value the blast furnace slag has a reverse effect on these properties.
- There is no a significant variation of the values of Σ for all used neutron energies by adding a different percentage of slag as a fine aggregate in concrete.
- 20 wt % of blast furnace slag as a fine aggregate in concrete was the optimum percentage for the values of mass attenuation coefficients of the most investigated γ-ray energy lines in concrete maxis.

References

[1] Mohammed M. Al-Humaiqani, Ahmed B. Shuraim, and Raja Rizwan Hussain, "γ-Radiation Shielding Properties of High Strength High Performance Concretes Prepared with Different Types of Normal and Heavy Aggregates",Asian Transactions on Engineering, 3 (2), pp. 18-28, 2013.

[2] V. Fugarua, S. Bercea, C. Postolache, S. Manea, A. Moanta, I. Petre, and M. Gheorghe, "Gamma Ray Shielding Properties of Some Concrete Materials", ACTA PHYSICA POLONICA A, 147 (2), pp. 1427-1429, 2015.

[3] Kanwaldeep Singh, Sukhpal Singh, and Gurmel Singh, "Effect of Flyash Addition on Mechanical and Gamma Radiation Shielding Properties of Concrete", Hindawi Publishing Corporation Journal of Energy, 2014, pp. 1-7, 2014.

[4] El Shazly R.M., Kany A.M.I., Abd El-ghafar M., Sayed E.A., Hegazy F.E., and Kany M.S.M.I.: "Design of special type of heavy weight fiber concrete as radiation shielding medium", Isotope & Radiation Research Bulletin Issued by Middle Eastern Regional Radioisotope Centre for The Arab Countries, 39 (1), pp. 81-89, 2007.

[5] T. Piotrowski, D.B. Tefelski, J.J. Sokołowska, and B. Jaworska, "NGS-Concrete — New Generation Shielding Concrete against Ionizing Radiation — the Potential Evaluation and Preliminary Investigation" , ACTA PHYSICA POLONICA A, 128 (2-B), pp. 9-13, 2015.

[6] Yung-Chin Ding, Ta-Wui Cheng, Ping-Chun Liu, and Wei-Hao Lee, "Study on the treatment of BOF slag to replace fine aggregate in concrete", Construction and Building Materials, 146, pp. 644–651, 2017.

[7] Hisham Qasrawi, "The use of steel slag aggregates to enhance the mechanical properties of recycled aggregate concrete and retain the environment", Construction and Building Materials, 54, pp. 298–304, 2014.

[8] C.R. Panda, K.K. Mishra, K.C. Panda, B.D. Nayak, and B.B. Nayak, "Environmental and technical assessment of ferrochrome slag as concrete aggregate material", Construction and Building Materials, 49, pp. 262–271, 2013.

[9] B.M. Mithun and M.C. Narasimhan, "Performance of alkali activated slag concrete mixes incorporating copper slag as fine aggregate", Journal of Cleaner Production, 112, pp. 837-844, 2016.
[10] Alan Richardson, Reuse of Materials and Byproducts in Construction, Green Energy and Technology, Springer-Verlag London, 2013.
[11] How-Ji Chen, Shao-Siang Huang, Chao-Wei Tang, M.A. Malek, and Lee-Woen Ean, "Effect of curing environments on strength, porosity and chloride ingress resistance of blast furnace slag cement concretes: A construction site study", Construction and Building Materials, 35, pp. 1063–1070, 2012.
[12] P. Sharmila and G. Dhinakaran, "Compressive strength, porosity and sorptivity of ultra fine slag based high strength concrete", Construction and Building Materials, 120, pp. 48–53, 2016.
[13] Aleksander Samarin, "Use of Concrete as a Biological Shield from Ionising Radiation", Energy and Environmental Engineering, 1(2), pp. 90-97, 2013.
[14] J. S. Lilley, Nuclear physics principle and applications, John Wiley & Sons, Ltd, 2002.
[15] Vishwanath P. Singh and N.M. Badiger, "Gamma ray and neutron shielding properties of some alloy materials", Annals of Nuclear Energy, 64, pp. 301–310, 2014.
[16] Burcu AKÇA and Salih Zeki ERZENEOĞLU, "Measurement of Linear Attenuation Coefficients of Compounds of Some Essential Major Elements", Journal of Multidisciplinary Engineering Science and Technology (JMEST), 3(6), pp. 5003-5006, 2016.
[17] Vishwanath P. Singh, M.E. Medhat, and S.P. Shirmardi, "Comparative studies on shielding properties of some steel alloys using Geant4, MCNP, WinXCOM and experimental results", Radiation Physics and Chemistry, 106, pp. 255–260, 2015.
[18] Aly Saeed, R.M. El shazly, Y.H. Elbashar, A.M. Abou El-azm, M.M. El-Okr, M.N.H. Comsan, A.M. Osman, A.M. Abdal-monem, A.R. El-Sersy, "Gamma ray attenuation in a developed borate glassy system", Radiation Physics and Chemistry, 102, pp. 167–170, 2014.
[19] Gerward, L., Guilbert, N., Jensen, K.B., Levring, H., "X-ray absorption in matter Reengineering XCOM", Radiat. Phys. Chem., 60, pp. 23–24, 2001.
[20] John R. Taylor, An Introduction to error analysis the study of uncertainties in physical measurements, second edition, University science books, Sausalito, California, 1982.
[21] Mosaad Mohamad Sadawy, "Effect of Al_2O_3 additives on the corrosion and electrochemical behavior of steel embedded in ordinary Portland cement concrete", American Journal of Materials Research, 1(4), pp. 53-58, 2014.
[22] Elie Kamseu, Chiara Ponzoni, Chayanee Tippayasam, Rosa Taurino, Duangrudee Chaysuwan, Maria Chiara Bignozzi, Luisa Barbieri, Cristina Leonelli, "Influence of fine aggregates on the microstructure, porosity and chemico-mechanical stability of inorganic polymer concretes", Construction and Building Materials, 96, pp. 473–483, 2015.